Robust Control in 4x4 Hybrid-converted Touring Vehicles During Urban Speed Steering Maneuvers

Rafael C. B. Sampaio, Marcelo Becker, Vinicius L. Lemos, Adriano A. G. Siqueira,
Jussara Ribeiro, Glauco A. P. Caurin
University of São Paulo - EESC - Mechatronics Lab - São Carlos/SP, Brazil - 13566-590
Email: rafaelc@sc.usp.br, becker@sc.usp.br, vl-lemos@uol.com.br, siqueira@sc.usp.br,
jussara.jsr@gmail.com, gcaurin@sc.usp.br

***Abstract*—The present work is focused on the synthesis and the analysis of robust control techniques for rear electric traction control in 4X4 hybrid-converted CVs (Conventional Vehicles) at urban speed limits (lower than 60 Km/h). This set represents a practicable alternative for the automotive industry, improving vehicular performance and reducing considerably fossil fuel air pollution. Our goal is to design an electromechanical controlled system that can replace the conventional rear wheels in touring cars with a pair of electric wheels with a minimal level of adaptation, preserving the original combustion engine. We consider the synthesis of an H_∞ robust controller and also the neurofuzzy approach. An optimized PID controller was also designed for the final analysis and evaluation. Based on Ackerman Geometry and the reading of the steering front angles, it was possible to estimate the maneuver radius from turning center. Thus, all three proposed control approaches must adjust the rear wheel's individual angular speeds by means of the current control of the two electrical motors linked to them, so that the car presents an appropriate behavior during all possible maneuvers. Finally, computation models were run in order to compare the three controllers.**

I. Introduction

The hybrid vehicle concept fills a huge demand for new transportation facilities which could significantly reduce emissions from motor vehicles. For example, over their entire full cycle, PHEVs (Plug-in Hybrid Electric Vehicles) emits less CO_2 than CVs (Conventional Vehicles) and HEVs (Hybrid Electric Vehicles) [1]. The hybridization of the drive trains in public transportation associated with the use of supercapacitors as an ESS (Energy Storage System) could recover up to 40% of the energy when they break [2]. Many previous works often treat the design of electrical/hybrid vehicles focused on unpublished or inedited conceptions, which are often built up entirely from a "blank desk". Our goal is to design a full controlled electromechanical device that can be perfectly adapted to preexisting touring cars, without great structural adaptations. In order to have an wide overview of the control possibilities, we consider the use of three approaches. The first one refers to an optimized PID controller, whose recurrence equations have been drastically modified to improve performance [3]. The second one considers the synthesis of an H_∞ robust controller based in the general robust control theory [4], [5]. Although there are many practicable modern solutions for this dynamic problem, control complexity increases as the contour conditions and project requirements raise, which implies a very significant process cost growth [6]. Thus, we consider, as third approach, the design of an artificial intelligence-based controller, which is supported by the idea of combining fuzzy logic ease in abstracting knowledge and the low process cost that the neural networks demand, generating neurofuzzy systems [7] that combine the advantages of those two paradigms [8]. A FLC (Fuzzy Logic Controller) was designed [9] prior to the design of the neural network [10]. The four-layered feedforward neural network analysis is strongly followed [11]. A simplified dynamic model of the vehicle is presented [12] and some relations were developed based on Ackerman Geometry, from which individual rear wheels angular speeds are determined, so that all maneuver stability levels could be accomplished [13]. Traction system considers the identification of two 5HP electrical DC motors, in their respective space state representation, modeled based on experimental techniques [14].

II. Electric Wheels Control Problem Formulation

The vehicle modeled in this work consists of a conventional touring car, driven by a conventional combustion engine for the frontal traction. Once our electromechanical device can properly replace both conventional rear wheels, we can treat the original car as an hybrid vehicle indeed. In our case, only the rear electric wheels shall operate at general urban speed limits (lower than 60 Km/h), so that the combustion engine must be inoperative. Above of this speed, the conventional combustion engine assumes the traction system and the electric rear device is then decoupled. Figure 1 shows the hybrid vehicle architecture. The steering angles and the vehicle speed are available from the CAN bus network (A). These data are sent to our boarding computer which calculates the correct reference values (B). The two electric wheels are then controlled by means of electrical current control (C), so that the measured angular speeds of the wheels are in compliance to the reference values, thus stability in maneuvers is guaranteed.

A. Vehicle Modeling

We based the vehicle's dynamic model on a simplified 2D version [12]. It considers all geometric relations intrinsic to a four wheel touring car, with front steering system, as it can be observed in Fig. 2. We have $\delta_{1,2}$ as the steering

978-1-4244-8218-4/10/$26.00 ©2010 IEEE

angles, $\beta_{1,2}$ are the angles between movement and rolling directions. The wheelbase is given by L, while l_1 and l_2 are, respectively, the distance between center of gravity and front and rear tracks. The distance between C.G. and turn center is given by R_{cg}, while R is the distance between turn center and rear track mean length. The track length is denoted by b. Variables R_1 and R_2 are the distances between turn center and left and right wheels, respectively. Forward and angular velocities are respectively denoted by V_{cg} and ω_z, both with respect to C.G. Variables $U_{1..4}$ represent the longitudinal forces along the steering angle direction. Transversal forces along the four wheels are given by $S_{1..4}$. The power that the combustion engine transmits to both front left and right wheels are represented by $P_1(t)$ and $P_2(t)$, respectively. The power that the electric motors transmit to the left and right rear wheels are given by $P_3(t)$ and $P_4(t)$, espectively.

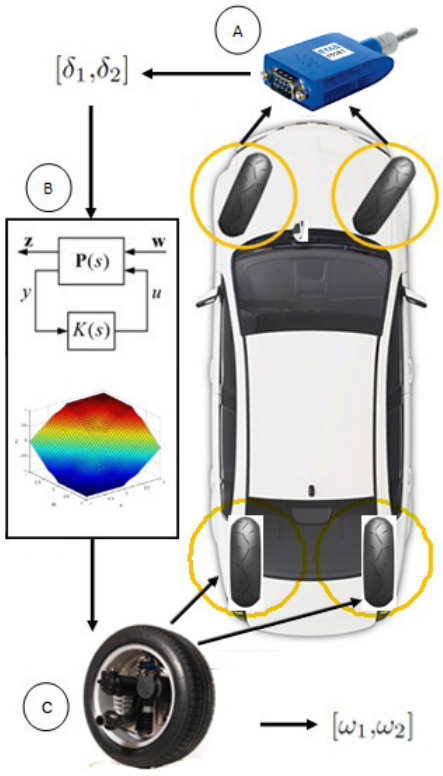

Fig. 1: Control architecture of the hybrid-converted vehicle.

Sketching the free body diagram referent to Fig. 2, we achieve the following equations, which describe the dynamics of the vehicle:

$$\dot{V}_x = \frac{1}{m}\left(U_3 + U_4 - S_1 cos\beta_1 - S_2 cos\beta_2\right) + V_y\omega_z \quad (1)$$

$$\dot{V}_y = \frac{1}{m}\left(S_3 + S_4 + S_1 sin\beta_1 + S_2 sin\beta_2\right) - V_x\omega_z \quad (2)$$

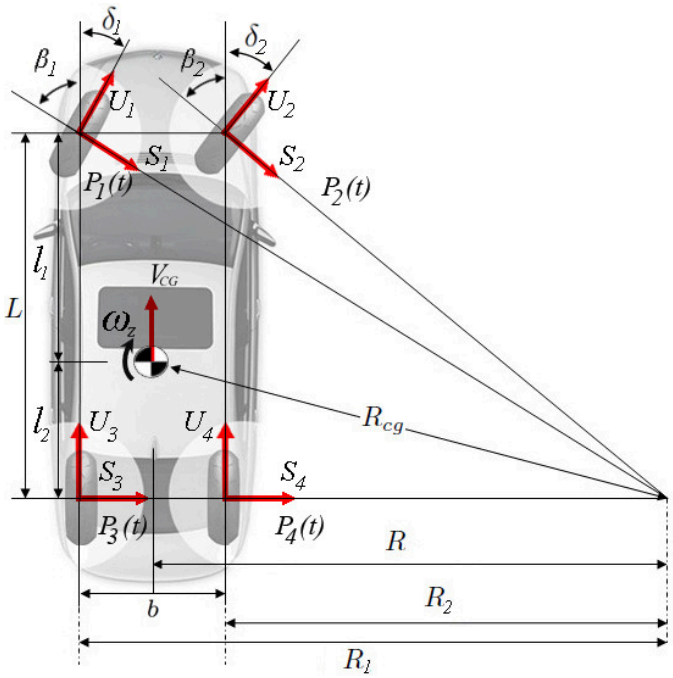

Fig. 2: Steering kinematics through which Ackerman Geometry is achieved.

$$\dot{\omega_z} = \frac{1}{I_z}\left[\frac{b}{2}(U_3 - U_4) - l_2\left(S_3 + S_4\right) + l_1\left(S_1 sin\beta_1 - S_2 sin\beta_2\right) + \frac{b}{2}\left(S_2 cos\beta_2 - S_1 cos\beta_1\right)\right] \quad (3)$$

Where I_z is the moment of inertia over z axis and m is the mass of the vehicle. The longitudinal forces that act over the wheels are:

$$U_1 = U_2 = -\frac{\mu m g l_2}{2L} \quad (4)$$

$$U_3 = \frac{P_3(t)}{(V_x + \frac{b}{2}\omega_z)} - \frac{\mu m g l_1}{2L} \quad (5)$$

$$U_4 = \frac{P_4(t)}{(V_x - \frac{b}{2}\omega_z)} - \frac{\mu m g l_1}{2L} \quad (6)$$

Where μ and g are, respectively, the coefficient of friction and the gravitational acceleration. As in our case study only $P_3(t)$ and $P_4(t)$ are considered, the resultant forces $U_{1,2}$ are the opposite forces due to friction. Transversal forces are given by:

$$S_1 = C_{\psi F}\left(\delta_1 - \frac{V_y + l_1\omega_z}{V_x + \frac{b}{2}\omega_z}\right) \quad (7)$$

$$S_2 = C_{\psi F}\left(\delta_2 - \frac{V_y + l_1\omega_z}{V_x - \frac{b}{2}\omega_z}\right) \quad (8)$$

$$S_3 = -C_{\psi T}\left(\frac{V_y - l_2\omega_z}{V_x + \frac{b}{2}\omega_z}\right) \tag{9}$$

$$S_4 = -C_{\psi T}\left(\frac{V_y - l_2\omega_z}{V_x - \frac{b}{2}\omega_z}\right) \tag{10}$$

Where C_ψ is the slip coefficient, and the subindices T and F stand for rear and front wheels, respectively. According to [13], aiming the appropriated behavior in turns, front wheel angles must follow the Ackerman Geometry, given by:

$$\delta_1 = arctg\left(\frac{L}{R_{cg} + \frac{b}{2}}\right) \approx \left(\frac{L}{R_{cg} + \frac{b}{2}}\right) \tag{11}$$

$$\delta_2 = arctg\left(\frac{L}{R_{cg} - \frac{b}{2}}\right) \approx \left(\frac{L}{R_{cg} - \frac{b}{2}}\right) \tag{12}$$

Once we know the vehicle's speed and the steering angles, considering the vehicle as a rigid body and performing several geometric relations, we achieve the following equations, which safely represent, the rear angular speeds of the right and left wheels, which must be correctly adjusted by the controller:

$$\omega_1 = \frac{V_{cg}}{rR_{cg}}\left[\sqrt{R_{cg}^2 - l_2^2} + \frac{b}{2}\right] \tag{13}$$

$$\omega_2 = \frac{V_{cg}}{rR_{cg}}\left[\sqrt{R_{cg}^2 - l_2^2} - \frac{b}{2}\right] \tag{14}$$

Where r is the radius of the pneumatic.

B. DC Motor Modeling

We considered the characterization of two 5 HP DC motor for the vehicle's rear traction system. This process was based on experimental procedures which allow us to obtain all electromechanical parameters for obtaining the transfer function for the analysis. In order to ease computation and expedite calculation involving transfer matrices, we consider the DC motor model representation in the packed form [5], using all parameters previously determined in our experiments, which is given by:

$$G(s) = \left[\begin{array}{cc|c} -120 & -700 & 1 \\ 1 & 0 & 0 \\ \hline 1 & 50 & 0 \end{array}\right] \tag{15}$$

III. Control Design

A. PID Controller Recurrence Equations

The digital PID controller consists on the modified recurrence equations proposed in [3]. It considers the positional form with backward difference approximation to the integrative term (I) and *Tustin* approximation to derivative term (D), whose control laws can be respectively represented by:

$$P(k) = K_p[\beta r(k) - y(k)]; \tag{16}$$

$$I(k) = I(k-1) + \frac{K_p T}{T_i}e(k-1) \tag{17}$$

$$D(k) = \frac{2T_d - TN}{2T_d + TN}D(k-1) + \frac{2K_pT_dN}{2T_d + TN}(y(k) - y(k-1)) \tag{18}$$

T is the sample rate of data acquisition, N is the optimization parameter for derivative action. β is the fine tuning parameter for proportional action, acting over the output signal [3]. Controller fine tunning followed $2nd$ Ziegler-Nichols method until the best value for proportional, derivative and integrative gains were reached.

B. Synthesis of the H_∞ Robust Control

The H_∞ controller designed was based on the work of [4] and [5]. The controlled process is a feedback SISO system, where the plant G is now represented by its augmented plant G_{ap}, seen from Fig. 3, where w is the input and z_1 and z_2 are the outputs. The goal is to find a H_∞ controller K whose closed-loop transfer matrix norm, between T_{zw} and $z_{1\ldots2}$, can be given by:

$$T_{wz} = \left\| \begin{array}{c} W_1S \\ W_2KS \end{array} \right\|_\infty = \left\| \begin{array}{c} W_1S \\ W_2R \end{array} \right\|_\infty < 1 \tag{19}$$

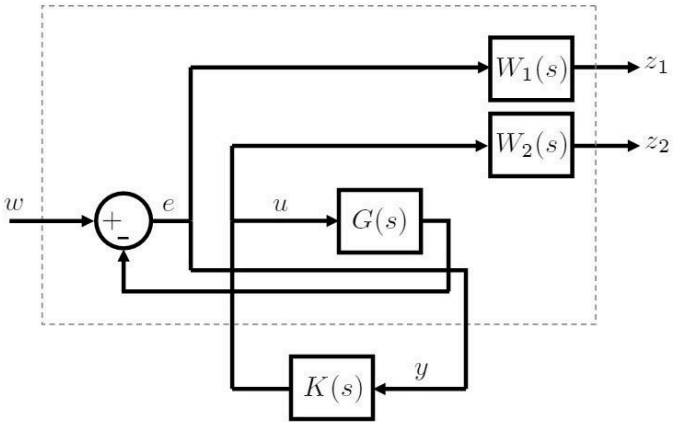

Fig. 3: Linear fractional transformation of the augmented plant matrix.

Where $W_{1,2}$ represent controller weighting functions.

Mixed sensitivity problem was considered, which is one of the H_∞ focus. In this context, S is sensitivity function while R is input sensitivity function, given by:

$$S = (I + L)^{-1} \tag{20}$$

$$R = K(I + L)^{-1} \tag{21}$$

Where L is the system open-loop transfer function written as:

$$L = GK \tag{22}$$

Both sensitivity and input sensitivity functions denote system robustness relative to disturbances rejection. It is necessary that the gains of R are low at high frequencies so that

noises/disturbances rejection can be guaranteed. On the other hand, S gains must be low at low frequencies to achieve the same rejection. Singular values analysis also are a good indicative of the robustness of the system against noises and disturbances in general.

It is essential to select the weight matrices properly for W_i, so that Eq. (19) can provide the system with robust control actions, satisfying project demands related to the electric wheels angular speed control, which are: 1) stability against model parametric variations, 2) stationary error $\rightarrow 0$, 3) robustness even with open-loop uncertainties and variations, 4) robustness against noises which are inserted into the plant.

1) Weighting Functions We and Wu Estimation Process: H_∞ weighting functions estimation is a quite complex process that not rarely demands iterative algorithms and does not exist a direct and specific formulation to achieve this goal. From the classic control theory, speed response is proportional to natural frequency ω_n and *overshoot* is determined by damping ratio ξ. As the desired performance is directly related to the sensitivity function, we consider ω_n and ξ directly related to sensitivity functions [5], given by:

$$S = \frac{s(s + 2\xi\omega_n)}{s^2 + 2\xi\omega_n s + \omega_n^2} \tag{23}$$

Although it is possible, from time domain, to calculate their corresponding parameters in frequency domain in therms of bandwidth ω_b and peak sensibility M_s, we analyze only the steady-state error with respect to a step input signal whose value is given by ϵ and that allows the choice of W_e function which satisfies the condition $|W_e(0)| \geq 1/\epsilon$, so that $\|W_e S\|_\infty \leq 1$ [5]. Maximum gain M_u of KS can assume high values while high frequencies gain is limited by bandwidth ω_b and sensor frequencies, for instance. In order to attenuate those frequencies, it is desired to reach values beyond the desired control band. In other words, it is necessary to find the singular values of $|S(j\omega)|$ (W_e) and $|KS(j\omega)|$ (W_u) functions for the H_∞ controller. Both weighting functions obtained are given by Eqs. (24) and (25) as follows:

$$W_e(s) = \frac{0.00625s + 50}{s + 0.05} \tag{24}$$

$$W_u(s) = \frac{s + 1}{0.1s + 9 \cdot 10^8} \tag{25}$$

From Eqs. (24) and (25) and all previous described procedures, the following controller K is achieved:

$$K(s) =$$

$$\frac{7.104(s + 9 \cdot 10^9)(s + 113.8)(s + 6.192)}{(s + 2018)(s + 0.05)(s^2 + 1515s + 3.061 \cdot 10^6)} \tag{26}$$

K controller frequency response can be seen through Fig. 4. Bode diagram turns it possible to analyze stability, which guarantees that the system is stable for a wide range of frequencies (and, then, conditions), considering the presence of noises/disturbances.

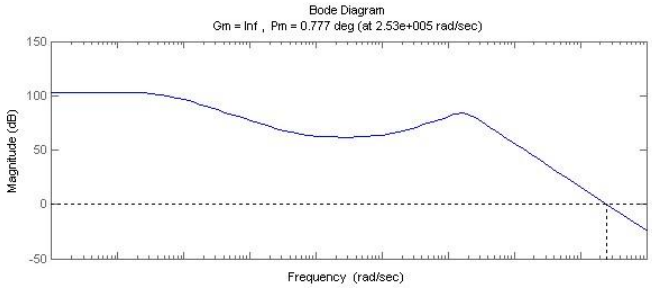

Fig. 4: Bode diagram of the H_∞ robust controller.

C. Neurofuzzy Approach

1) Fuzzy Controller Set Up: A fuzzy controller was designed inspired in [9], considering two inputs and one output. The input is represented by the two wheels angular speeds tracking errors E and their derivatives dE. In the other hand, output variable is given by the control action dU. Both E and dE utilize the following linguistic variables: Z set indicates that E and dE are at an acceptable zone. PL and NL respectively indicate that E and dE are positive and negative, with large margin of error. PM and NM respectively indicate that E and dE are positive and negative, with medium margin of error. Finally, PS and NS respectively indicate that E and dE are positive and negative, with small margin of error. As for the output, control action dU can be either an increase (PS, PM and PL) or a decrease (NS, NM and NL) in control signal. The FLC was provided with 49 rules, as can be seen from the look-up table in Fig. 5.

dE

E \ dE	NL	NM	NS	Z	PS	PM	PL
NL	NL	NL	NL	NL	NM	NS	Z
NM	NM	NM	NM	NM	NS	Z	PS
NS	NL	NM	NS	NS	Z	PS	PM
Z	NM	NM	NS	Z	PS	PM	PM
PS	NM	NS	Z	PS	PS	PM	PM
PM	NS	Z	PS	PM	PM	PM	PL
PL	Z	PS	PM	PL	PL	PL	PL

dU

Fig. 5: Fuzzy rules look-up table.

2) Feedforward Neural Network Design: A feedforward neural network was designed in order to replace fuzzy controller previously set up. A four-layered feedforward neural network with $(N/2) + 3$ hidden units was initially designed, once this set up is superior to a three-layered feedforward network in terms of the number of parameters needed for the training data [11]. The complete four-layered neural network architecture is shown in Fig. 6 [10].

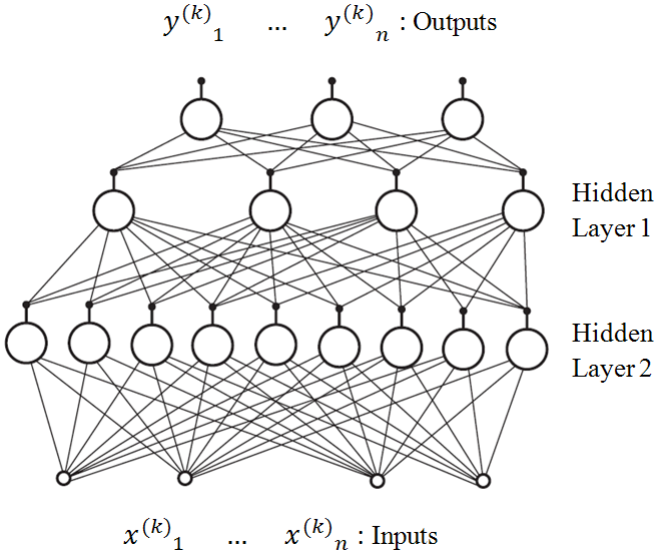

Fig. 6: Four-layered feedforward neural network architecture.

In our case, the neural network consists of a pair of inputs $x = (x_1^{(k)}, x_2^{(k)})$, which are the fuzzy controller input variables E and dE, respectively. Network single output consists of $y = y_1^{(k)}$ which refers to the fuzzy output variable given by dU. The idea is to provide the four-layered feedforward network with the vector containing E and dE as well as the desired output control signal dU. A Levenberg-Marquard algorithm was run and the training performance complied with MSE (Mean Square Error). Finally, the network evaluation process consist of the fuzzy control surface reconstruction process. The just designed neural network shall reconstruct the control surface, generated as the result of the fuzzy inference procedure. Figure 7 shows, at the left hand (A), the surface generated after the fuzzy inference process. At the right hand (B), the neural network reconstructs the fuzzy surface. This is the prove that ensures that the feedforward neural network is perfectly capable to provide the same control actions dU just as the fuzzy controller would do.

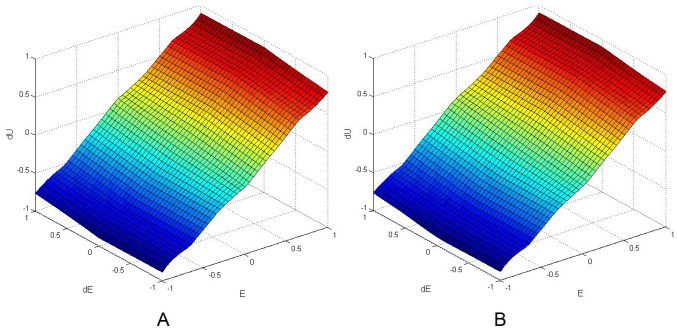

Fig. 7: FLC control surface obtained through the fuzzy rules (A) and the same control surface reconstructed by the the feedforward neural network (B).

IV. Results and Performance Evaluation

Both H_∞ and neurofuzzy controllers were subject of tests of changes in angular speed demands. Gaussian noise was also incorporated to the plant in order to evaluate the ability of controller related to noise/disturbances rejection.

Figure 8 illustrates the responses of all controllers while the vehicle is traveling, liable to maneuvers. It is noted that H_∞ controller presents a high ability to reject noises/disturbances. Although neurofuzzy ability to reject noises can't be compared to the H_∞ approach, the neurofuzzy controller presents an acceptable tracking error at the first second and then sustains the requested reference inputs.

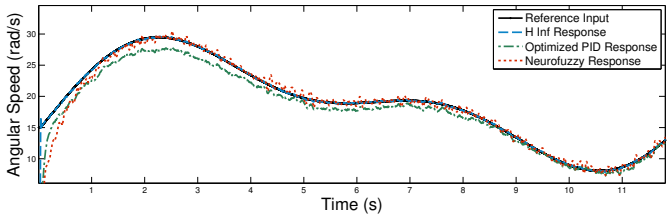

Fig. 8: Control responses during maneuvers, while vehicle is susceptible to changes in wheel speed reference values.

Figure 9 shows the controller responses to abrupt variations in speed amplitude, in order to evaluate some important characteristics of the vehicle performance, just as rising time, overshoot percent and steady state response. As for these three items, H_∞ has responded with minimum rising time, acceptable overshoot level and excellent steady state response. Neurofuzzy controller behavior is also efficient as for the rising time, and steady state response can also be considered acceptable. For this essay, PID controller performance is considered inefficient for brusque change in operation conditions. Actually, PID controller can't ensure robustness in all operation conditions. Figure 10 shows the breaking test results. Once again PID steady state error can't be neglected. In the other hand, H_∞ and neurofuzzy controllers have successfully accomplished this essay.

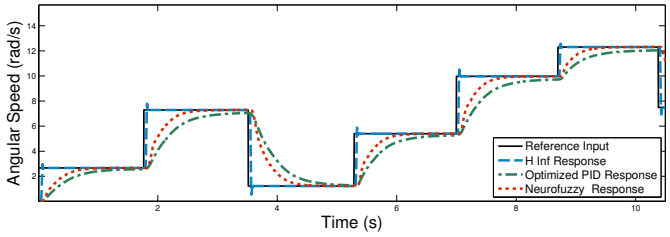

Fig. 9: Control responses for abrupt variations in reference speed amplitude.

Control effort is also a strong indicative for controller robustness. In this case, H_∞ (Fig. 11) and neural (Fig. 12) controllers efforts are highly varying, as soon as the speed of reference is provided, whereas the PID controller settles with

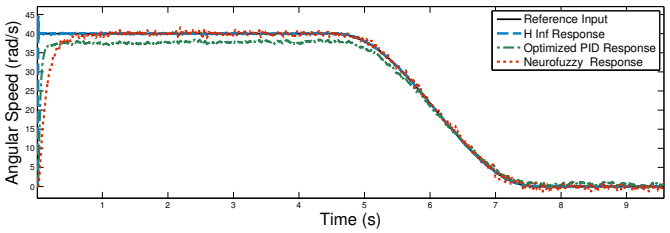

Fig. 10: Control responses for a breaking scenario.

steady error (13). Figure 14 also illustrates an abrupt change in speed demand, where the vehicle is initially parked. Again, the efforts of both H_∞ and neurofuzzy controllers are notable.

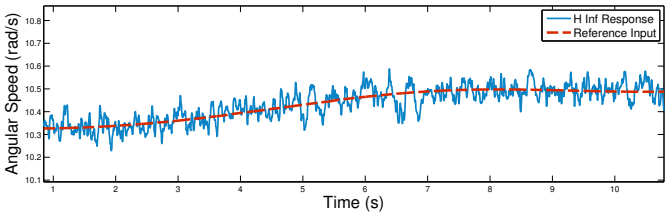

Fig. 11: Control effort with H_∞ controller.

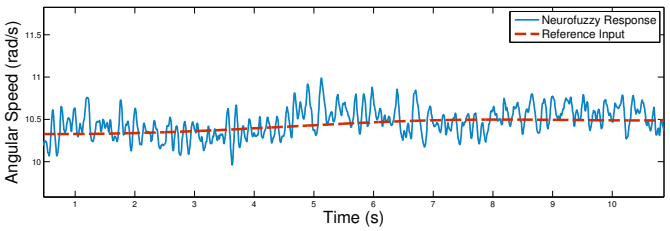

Fig. 12: Control effort with neurofuzzy controller.

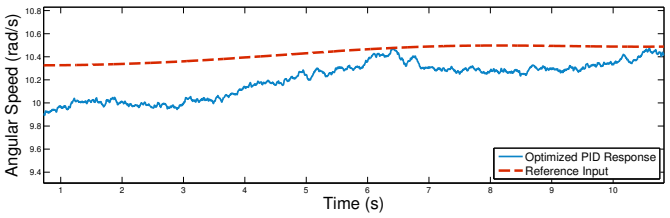

Fig. 13: Control effort with PID optimized controller.

V. Conclusions and Future Works

Both H_∞ and neurofuzzy controllers have produced good results at different simulation conditions. Thus, we could prove that modern control techniques, when well-designed, can provide excellent control responses so that the electric wheel speed control problem can be satisfactorily solved. In the other hand, we also proved that the neurofuzzy approach also provides excellent control actions for the problem. In other words, both approaches advantages make the hardware control architecture conception very flexible. In spite of the optimization process of the PID controller, it was definitely proved that the classic approach is not sufficiently versatile to such problem in comparison to the two previous controllers.

A reduced scale vehicle is being assembled at São Carlos School of Engineering/USP, in which the H_∞ and the neurofuzzy controllers will be properly embedded at the end of the first half of 2010.

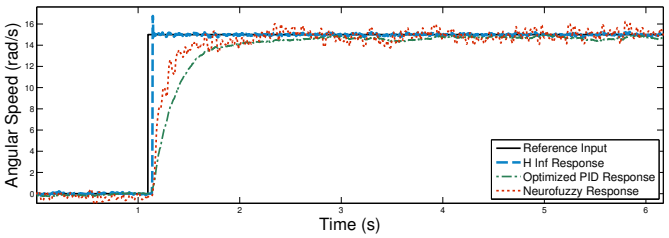

Fig. 14: Control effort for an abrupt change in reference speed amplitude with disturbances applied to the plant.

Acknowledgment

This work is supported by Brazilian Electricity Regulatory Agency (ANEEL), Compania Paulista de Forca e Luz (CPFL) and Fundação para o Incremento da Pesquisa e do Aperfeiçoamento Industrial (FIPAI).

References

[1] Sioshansi, R., Denholm, P., *Emissions impacts and benefits of plug-in hybrid electric vehicles and vehicle-to-grid services*, Environmental Science and Technology, 2009, 43, 1199 - 1204

[2] Barrero, R., Mierlo, J., Tackoen, X., *Energy savings in public transport*, Vehicular Technology Magazine, IEEE, 2008, 3, 26 -36

[3] Sampaio, R. C. B., Becker, M., *Mechatronic Servo System Applied To A Simulated-Based Autothrottle Module*, 20th International Congress of Mechanical Engineering, 1-10, 2009

[4] Doyle, J. C., K. Glover, P. P. K. and Francis, B. A, *State-space Solutions to Standard H_2 and H_∞ Control Problems*, Vol. 34, 1989

[5] Zhou, K., *Essentials of Robust Control*, Prentice Hall, 1997

[6] Kumar, M. V., Suresh, S., Omkar, S.N., Ganguli R., Sampath, P., *A Direct Adaptive Neural Command Controller Design for an Unstable Helicopter*, Journal of Engineering Applications of Artificial Intelligence, Elsevier Science, Oxford, 2009

[7] Cai, L., Rad, A., Chan, W. L., *An Intelligent Longitudinal Controller for Application in Semiautonomous Vehicles Industrial Electronics*, IEEE Transactions on, 57, 1487-1497, 2010

[8] Cirstea, M., Dinu, A., Khor, J. G., McCormick, M., *Neural and Fuzzy Logic Control of Drives and Power Systems*, 3rd CTA-DLR Workshop on Data Analysis & Flight Control, 2002

[9] Yager, R. R., Filev, D. P., *Essentials of Fuzzy Modeling and Control*, Chapter 4, Wiley-Interscience, New York, 1994

[10] Kurosawa, K., Futami, R., Watanabe, T., Hoshimiya, N., *Joint Angle Control by FES Using a Feedback Error Learning Controller Neural Systems and Rehabilitation Engineering*, IEEE Transactions on Neural Systems and Rehabilitation Engineering, 13, 359-371, 2005

[11] Tamura, S., Tateishi, M., *Capabilities of a Four-Layered Feedforward Neural Network: Four Layers Versus Three*, IEEE Transactions on Neural Networks, Vol. 8, 2, 1997

[12] Becker, M. *Estudo sobre Robos de Locomocao: Formas Construtivas, Dirigibilidade e Controle*, MSc. Thesis, UNICAMP, 1997

[13] Gillespie, T. D., *Fundamentals of Vehicle Dynamics*, SAE International, 1992

[14] Levine, W. S., *Control System Fundamentals*, CRC Press, Inc., Boca Raton, FL, 1999